A six-degree-of-freedom robotic motion system for quality assurance of real-time image-guided radiotherapy

To cite this article before publication: Saree Alnaghy *et al* 2019 *Phys. Med. Biol.* in press https://doi.org/10.1088/1361-6560/ab1935

A six degree-of-freedom robotic motion system for quality assurance of real-time image-guided radiotherapy

Saree Alnaghy

E-mail: saree@uow.edu.au
ACRF Image X Institute, The University of Sydney Central Clinical School, Sydney, NSW, Australia

Andre Kyme

School of Aerospace, Mechanical, and Mechatronic Engineering, University of Sydney, Sydney, NSW, Australia

Vincent Caillet

ACRF Image X Institute, The University of Sydney Central Clinical School, Sydney, NSW, Australia
Northern Sydney Cancer Centre, Royal North Shore Hospital, Sydney, New South Wales, Australia

Doan Trang Nguyen

ACRF Image X Institute, The University of Sydney Central Clinical School, Sydney, NSW, Australia

Ricky O'Brien

ACRF Image X Institute, The University of Sydney Central Clinical School, Sydney, NSW, Australia

Jeremy T. Booth

Northern Sydney Cancer Centre, Royal North Shore Hospital, Sydney, New South Wales, Australia
Institute of Medical Physics, School of Physics, The University of Sydney

Paul J. Keall

E-mail: paul.keall@sydney.edu.au
ACRF Image X Institute, The University of Sydney Central Clinical School, Sydney, NSW, Australia

Abstract. In this study we develop and characterise a six degree-of-freedom (6DoF) robotic motion system for quality assurance of real-time image-guided radiotherapy

techniques. The system consists of a commercially available robotic arm, an acrylic phantom with embedded Calypso markers, a custom base plate to mount the robot to the treatment couch, and control software implementing the appropriate sequence of transformations to reproduce measured tumour motion traces. The robotic motion system was evaluated in terms of the set-up and motion trace repeatability, static localization accuracy and dynamic localization accuracy. Four prostate, two liver and three lung motion traces, representing a range of tumor motion trajectories recorded in real patient treatments, were executed using the robotic motion system and compared with motion measurements from the clinical Calypso motion tracking system. System set-up and motion trace repeatability was better than 0.5 deg and 0.3 mm for rotation and translation, respectively. The static localization accuracy of the robotic motion system in the LR, SI and AP directions was 0.09 mm, 0.08 mm and 0.02 mm for translations, respectively, and 0.2°, 0.06° and 0.06° for rotations, respectively. The dynamic localization accuracy of the robotic motion system was <0.2 mm and <0.6° for translations and rotations, respectively. Thus, we have demonstrated the ability to accurately mimic rigid-body tumor motion using a robotically controlled phantom to provide precise geometric QA for advanced radiotherapy delivery approaches.

Keywords: Six degrees of freedom; Intrafraction motion; Quality assurance; Robotic motion; Motion-adaptive radiotherapy

1. Introduction

Modern radiotherapy systems aim to deliver an accurate radiation dose to the clinical target volume (CTV) while sparing healthy tissue. However, this is easily confounded by tumour motion resulting from both whole-body movement during patient setup procedures and inter and intrafraction organ motion. In stereotactic body radiation therapy (SBRT), high doses are delivered in few fractions within a small field size, making motion management particularly important.

Real-time image-guided radiotherapy (IGRT) is used to treat localized tumors by compensating for tumor movement online during radiation delivery. A variety of commercial IGRT systems are currently being used to treat patients and compensate for tumor motion during delivery. These include CyberKnife Synchrony (Galal *et al* 2016) (Accuray, Sunnyvale, CA), MHI Vero tracking gimbaled linear accelerator (linac) (Depuydt *et al* 2014) (Mitsubishi Heavy Industries, Ltd., Japan and BrainLAB AG, Feldkirchen, Germany), Calypso (Kupelian *et al* 2007) (Varian, Palo Alto, CA), and MRIdian (Viewray, Oakwood, OH) (Mutic and Dempsey 2014), with an increasing number of systems at the research and development stages. For example, Kilovoltage Intrafraction Monitoring (KIM) uses gold fiducial markers implanted inside a tumor to estimate the tumor location based on X-ray images of the target (Keall *et al* 2015). This enables motion in the left-right (LR), superior-inferior (SI), anterior-posterior (AP), roll, pitch and yaw directions to be determined. Markerless tumor tracking is also being investigated (Shieh

et al 2015, Sörnsen de Koste *et al* 2015).

Multi-leaf collimators (MLC) have been implemented as a real-time motion adaptation technique on standard linacs, allowing the beam to be shifted to track tumor motion (Falk *et al* 2010). The first MLC-based tracking in a clinical trial was demonstrated in 2013 using electromagnetic-guided transponders implanted in the prostate (Keall *et al* 2016). Another recently developed technology enables precise patient positioning using treatment couches with six-degree-of-freedom (6DoF) motion capability (Gevaert *et al* 2012, Schmidhalter *et al* 2013, Schmidhalter *et al* 2014). Such systems include the gKteso 6DoF couch (gKteso GmbH, Bobingen, Germany), Elekta HexaPOD (Elekta, Stockholm, Sweden) and the Varian PerfectPitch couch. Robotic couch tracking systems have also been developed based on this technology and are undergoing clinical translation (Ehrbar *et al* 2017). These systems rely on a fixed radiation beam while moving the patient to compensate for tumor motion based on a real-time guidance system such as Calypso (Wilbert *et al* 2013). Recently, a 6DoF motion platform was developed to compensate for head movements during stereotactic radiosurgery and provide frameless and maskless treatment (Belcher *et al* 2014, Belcher *et al* 2017). The geometric accuracy and reproducibility of this system were evaluated using an anthropomorphic head phantom and an infrared optical tracking system.

Greater understanding of the dosimetric effects of rotational motion has driven the evolution and rising trend of IGRT technologies and robotic positioning systems. This in turn has brought about growth in rotational quality assurance (QA) devices. Ideally, a QA motion device should provide accurate replication of known 6DoF tumor motion in order to characterize the performance of IGRT delivery. However, the available QA devices are restricted in their range of motion and are therefore unable to fully replicate patient-measured 6DoF tumor motion. For example, the commercially available HexaMotion (HexaMotion^{TM}, Scandidos, Uppsala, Sweden) platform is limited to five degrees of freedom, with angular rotation restricted to $\pm 10^\circ$ and $+3^\circ/-6^\circ$ in the SI and LR directions, respectively, and no AP rotation. Larger angular flexibility is required to reproduce measured tumor motion, as prostate rotations $>15^\circ$ and lung tumor rotations $>45^\circ$ along the LR direction have been observed (Huang *et al* 2015, Plathow *et al* 2006).

In this paper, we present a 6DoF robotic motion system capable of reliably and reproducibly replicating the full range and rate of patient-measured tumor motion, and therefore suitable for QA of real-time IGRT techniques. The system uses a robotic arm to manipulate a custom-built phantom according to commanded input motion sequences. We describe the physical design of the system, the formulation of motion transformations to correctly replicate tumor motion, and the tests used to validate the system against the Calypso motion tracking system, a widely used, FDA-approved, clinical device that measures 6DoF target motion.

2. Materials and Methods

2.1. Robotic phantom

The robotic system comprised a 6-axis robot and custom-built phantom (figure 1). The UR3 robot (Universal Robots, Odense Denmark) was chosen for this application due to its position repeatability (±0.1 mm) and angular flexibility (±360° in all axes) (Robots 2015). The UR3 is fully programmable and supports a 3 kg payload at a reach of approximately 500 mm. This range allows the phantom to be extended into the treatment field without having any mechanical support below the phantom that may impact image quality during tracking. The polymethylmethacrylate (PMMA) phantom was manufactured with three embedded Calypso markers (Bell *et al* 2017). For these experiments we used three markers placed in a triangular formation (left, right and apex) according to standard clinical practice. The phantom was designed to be reproducibly attached to the robot arm. We designed a custom aluminum plate to mount the robot and rigidly attach it to the treatment couch during operation.

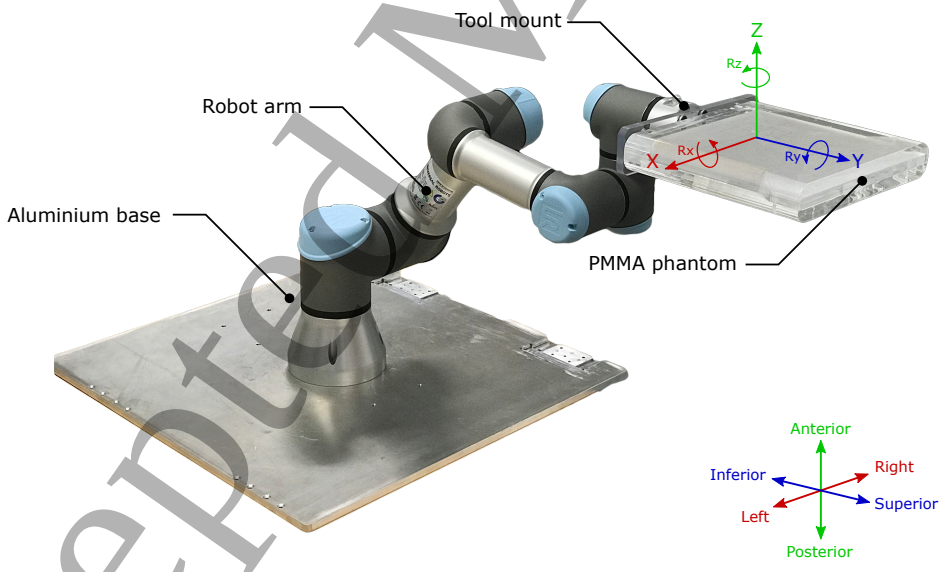

Figure 1. Prototype robotic motion system, depicting custom base mount and acrylic phantom. The phantom coordinate system is overlaid and is defined based on the IEC 61217 clinical protocol for radiotherapy equipment (see Section 2.2).

2.2. Coordinate transformations

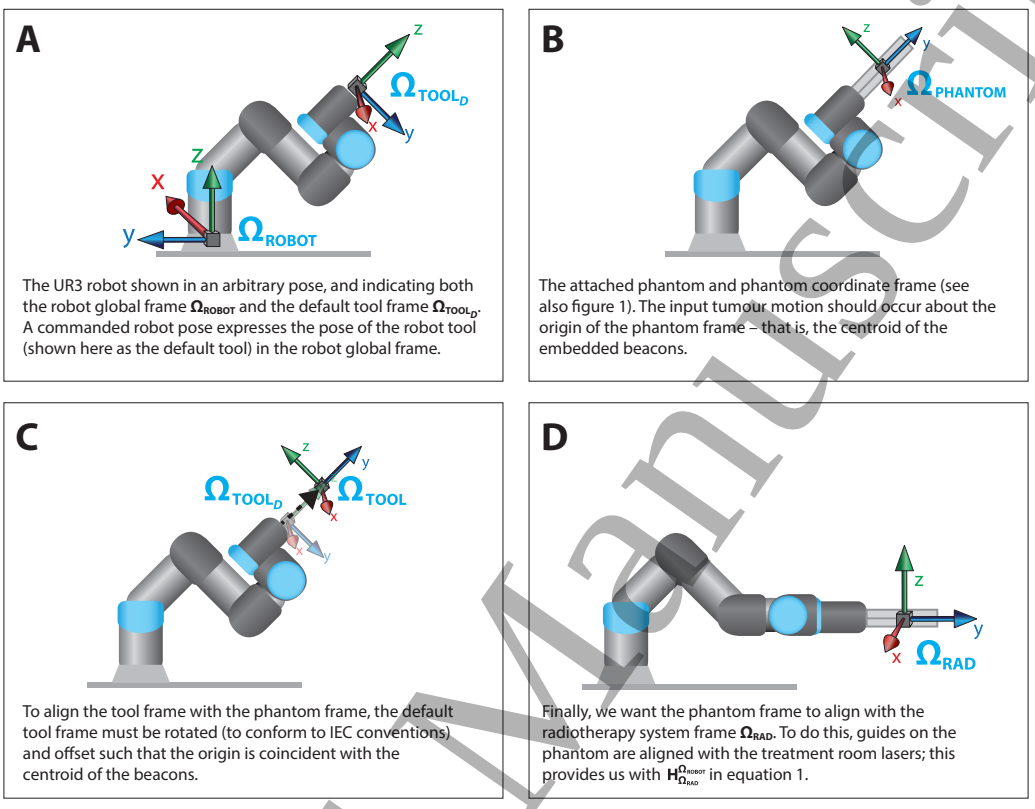

Figure 2. Robotic motion system coordinate systems, and coordinate transformations required to mimic recorded tumor motion.

The heart of the robotic motion system methodology consists in a series of coordinate transformations that allow input traces of tumour motion to be accurately reproduced by the robot in a relevant clinical frame. In order to understand the required transformations, we first define the main coordinate frames:

Robot global frame, $\mathbf{\Omega_{Robot}}$: This is the fixed (factory-defined) robot coordinate system with origin nominally at the centre of the robot base and axes defined as shown in figure 2A.

Robot tool frame, $\mathbf{\Omega_{Tool}}$: The tool refers to the rigidly mounted device at the end of the robotic arm which is manipulated within the environment. Commanded/reported robot poses describe the position and orientation of the tool in the robot global frame. Unlike $\mathbf{\Omega_{Robot}}$ which is fixed, the robot tool frame is arbitrary. The default tool is the flange of wrist 3 at the end of the UR3 arm, and the default tool frame - what we will denote $\mathbf{\Omega_{Tool_D}}$ - is defined with origin at the centre of the flange and axes as shown in figure 2A.

Phantom frame, $\mathbf{\Omega_{Phantom}}$: The phantom frame is defined according to figure 2B and has origin at the centroid of the embedded Calypso markers and axes aligned with the

edges of the phantom.

Radiotherapy system frame, $\mathbf{\Omega_{Rad}}$: The radiotherapy system frame (figure 2D) has origin at the isocentre (defined by the treatment room lasers) and axes conforming to the International Electrochemcial Commission (IEC) 61217 clinical protocol for radiotherapy equipment (Commission 2011).

The aim is to determine the "commanded" robot poses for the default tool that will: (i) correctly map input tumour motion to the phantom frame (figure 2B); (ii) align the phantom frame with the tool frame (figure 2C); and (iii) ensure the tool frame is coincident with the radiotherapy frame (figure 2D). Moreover, for convenience, a given motion trace should be executed identically in each experiment without the need to reproducibly mount the robot to the treatment couch each time.

Letting $\mathbf{H}^{\mathbf{\Omega}}_{\mathbf{A}}$, denote the 4×4 homogeneous transformation matrix describing the rigid-body pose of object $\mathbf{A}$ in coordinate system $\mathbf{\Omega}$, the commanded robot poses satisfying the above requirements are given by:

$$\mathbf{H}^{\mathbf{\Omega_{Robot}}}_{\mathbf{\Omega_{Tool_D}}} = \mathbf{H}^{\mathbf{\Omega_{Robot}}}_{\mathbf{\Omega_{Rad}}} \cdot \mathbf{H}^{\mathbf{\Omega_{Rad}}}_{\mathbf{\Omega_{Phantom}}} \cdot \mathbf{H}^{\mathbf{\Omega_{Phantom}}}_{\mathbf{\Omega_{Tool}}} \cdot \mathbf{H}^{\mathbf{\Omega_{Tool}}}_{\mathbf{\Omega_{Tool_D}}} \tag{1}$$

Each of the terms in (1) is explained below. $\mathbf{H}^{\mathbf{\Omega_{Tool}}}_{\mathbf{\Omega_{Tool_D}}}$ represents the mapping between the tool frame and default tool frame and is defined as:

$$\mathbf{H}^{\mathbf{\Omega_{Tool}}}_{\mathbf{\Omega_{Tool_D}}} = \begin{bmatrix} 1 & 0 & 0 & x \\ 0 & 0 & -1 & y \\ 0 & 1 & 1 & z \\ 0 & 0 & 0 & 1 \end{bmatrix} \tag{2}$$

where x, y and z are the component shifts characterising the 3D offset of the centroid of the Calypso beacons relative to the centre of the default tool, in the default tool frame $\mathbf{\Omega_{Tool_D}}$. The offsets function to shift the origin of the tool frame from the default tool origin to the centroid of the embedded beacons. The rotation component represents the transformation required to align the default tool coordinate axes with the IEC specification, consistent with both $\mathbf{\Omega_{Phantom}}$ and $\mathbf{\Omega_{Rad}}$.

$\mathbf{H}^{\mathbf{\Omega_{Phantom}}}_{\mathbf{\Omega_{Tool}}}$ represents the mapping between the phantom frame and tool frame. We construct the tool frame to be coincident with the phantom frame. Details on how this is implemented are outlined below in Section 2.3.

$\mathbf{H}^{\mathbf{\Omega_{Rad}}}_{\mathbf{\Omega_{Phantom}}}$ represents the input tumour motion we wish to apply to the phantom and which was originally measured in a clinical radiotherapy frame.

$\mathbf{H}^{\mathbf{\Omega_{Robot}}}_{\mathbf{\Omega_{Rad}}}$ represents the mapping between the robot global frame and the relevant clinical radiotherapy frame.

Finally $\mathbf{H}^{\mathbf{\Omega_{Robot}}}_{\mathbf{\Omega_{Tool_D}}}$ represents the mapping between the robot global frame and default tool; that is, it constitutes the "commanded" poses to be supplied to the robot controller which will cause the phantom to mimic the input physiological motion.

The sequence of transformations is represented graphically in figure 2. Conceptually, the combined sequence of transformations expressed in equation 1 allows us to generate a command pose $\mathbf{H}^{\mathbf{\Omega_{Robot}}}_{\mathbf{\Omega_{Tool_D}}}$, in the robot global frame, to manipulate the phantom about a standardised local coordinate system, with origin at the centroid of the embedded markers, and from any arbitrary starting pose of the phantom.

2.3. Implementation

(i) **Coordinate systems and transformation matrices**
In our implementation, all coordinate systems are right-handed and all 4×4 transformation matrices represent poses composed according to the sequence: x-axis rotation, y-axis rotation, z-axis rotation, and lastly translation.

(ii) **Determining $\mathbf{H}^{\mathbf{\Omega_{Tool}}}_{\mathbf{\Omega_{Tool_D}}}$**
In practice, a nominal value for $\mathbf{H}^{\mathbf{\Omega_{Tool}}}_{\mathbf{\Omega_{Tool_D}}}$ can be established based on the specifications of the phantom, the beacon placement, the bracket attaching the phantom to the default UR3 tool, and the default tool itself. However, we determined $\mathbf{H}^{\mathbf{\Omega_{Tool}}}_{\mathbf{\Omega_{Tool_D}}}$ experimentally by performing a computed tomography (CT) scan of the phantom and UR3 tool. The CT scan was acquired using a Phillips Brilliance system with 1 mm slice thickness and the data were reconstructed with Metal Artefacts Reduction for Orthopaedic Implants (O-MAR) to reduce streaking artefacts introduced by the robotic arm. The UR3 tool, phantom and beacons were all clearly visible in the reconstructed images. Interpolated estimates of the x, y and z offsets of the centroid of the Calypso beacons relative to the centre of the UR3 tool were obtained from the reconstructed images based on the known pixel dimensions and used to compose $\mathbf{H}^{\mathbf{\Omega_{Tool}}}_{\mathbf{\Omega_{Tool_D}}}$. Since the phantom was designed to attach reproducibly to the UR3, these offsets only needed to be determined once.

(iii) **Determining $\mathbf{H}^{\mathbf{\Omega_{Phantom}}}_{\mathbf{\Omega_{Tool}}}$**
Since the phantom mounts reproducibly to the UR3, $\mathbf{\Omega_{Phantom}}$ and $\mathbf{\Omega_{Tool}}$ are coincident by design. Therefore, this transformation is simply the identity in our implementation.

(iv) **Determining $\mathbf{H}^{\mathbf{\Omega_{Robot}}}_{\mathbf{\Omega_{Rad}}}$**
In principle, $\mathbf{\Omega_{Rad}}$ could be any arbitrary starting pose about which the motion will be executed. In practice, for QA testing we want to choose $\mathbf{\Omega_{Rad}}$ as the clinical frame in the radiotherapy suite, and to precisely align the UR3 tool to this frame. This was achieved using engraved lines along the sides and top of the PMMA

phantom which we manually aligned to the treatment room lasers (defining $\mathbf{\Omega_{Rad}}$) in the radiotherapy suite.

(v) **Robot mounting**
Reproducibility of mounting the base plate to the treatment couch or the robot to the base plate is not important in our implementation. This is because the phantom-to-UR3 attachment is reproducible (by design) and the alignment of the phantom to the lasers ensures that in every experiment the robot global frame is properly aligned to the radiotherapy frame. The repeatability of the laser alignment step is addressed in Section 2.4.1.

(vi) **Handling UR3 conventions**
The UR3 platform expresses three-dimensional rotations using axis-angle (rotation vector) format - that is, parameterised by a unit vector $\mathbf{n}$ representing the axis of rotation and a scalar α quantifying the magnitude of rotation. Therefore, it was necessary to convert $\mathbf{H}^{\mathbf{\Omega_{Robot}}}_{\mathbf{\Omega_{Rad}}}$ from axis-angle format to matrix format for use in equation 1, and, subsequently, to convert $\mathbf{H}^{\mathbf{\Omega_{Robot}}}_{\mathbf{\Omega_{Tool_D}}}$ from matrix format back to axis-angle format to command the robot. The conversion is straightforward and details can be found in (Bajd *et al* 2010).

2.4. Experimental configuration

The robotic motion system was rigidly mounted to the treatment couch using the method described in section 2.1 and positioned directly beneath the Calypso detector panel. The phantom was initially aligned parallel to the treatment room lasers with the centroid of the three markers coinciding with the treatment isocenter. Its position was then fractionally adjusted so that the Calypso signal read (0,0,0) in translation. This removes any systematic offset between the robotic system and Calypso motion tracking system during the tumour motion traces. The aligned position of the phantom was automatically recorded by our software to accurately re-position the phantom between experiments if required. Figure 3 shows the experimental setup of the robotic motion system for the geometric QA tests using the Calypso tracking system.

The QA tests were based on the performance evaluation of the Hexamotion QA phantom by Huang et al. (Huang *et al* 2017), which were derived from the American Association of Physics in Medicine Task Group 40 (TG40) and Task Group 142 (TG142) protocols (Kutcher *et al* 1994, Klein *et al* 2009*b*). The tests included system (i.e. setup and motion trace) repeatability, static localization accuracy, and dynamic localization accuracy.

2.4.1. System repeatability. The system repeatability of the robotic motion phantom was evaluated to determine how well we could set up the robot and manually align the phantom to the lasers to reproduce the same motion. We performed the manual set-up and alignment four independent times, and for each set-up executed a prostate, liver

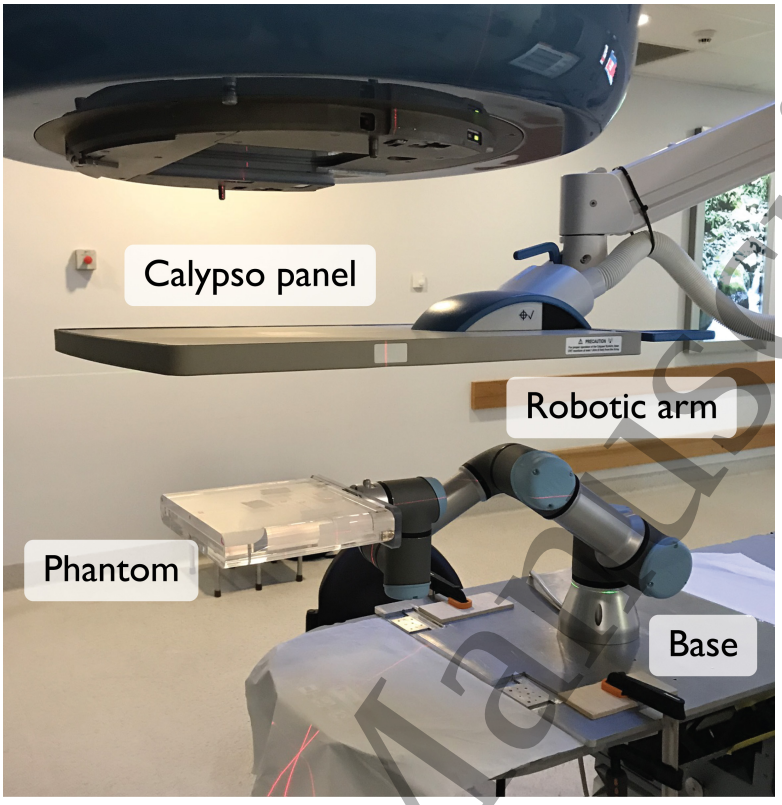

Figure 3. Experimental setup of the robotic motion system. The phantom is mounted to the Calypso treatment couch using a clamped base plate, and the phantom is then manually aligned to the treatment room lasers and treatment isocentre using the alignment engravings on the sides and top of the phantom.

and lung trace. The 6 DoF robot motion was sampled at 125 Hz using a real-time serial communication protocol (Modbus) (*Universal Robots, "Modbus Server - 16377"* n.d.). The maximum variance across the 4 repeat trials for each motion trace (prostate, liver, lung) was computed as a measure of repeatability.

2.4.2. Static localization accuracy. The static localization accuracy of the system was evaluated by moving the phantom to six translational poses (±40 mm in the LR, SI and AP directions) and six rotational poses (±10° around the LR, SI and AP directions). The commanded robot position was compared with the measured positions obtained using the Calypso tracking system. This process was repeated three times for each pose.

2.4.3. Dynamic localization accuracy. The dynamic localization accuracy of the system was estimated using selected prostate, liver and lung motion traces which are publicly available online (*ACRF Image X Institute,* Tumour motion (prostate, liver and lung) n.d.). Four prostate, two liver, and three lung 6DoF motion traces were implemented. These traces were chosen from over 200 traces to represent the spectrum of motion exhibited by tumors during treatment delivery. For the prostate, a slow-moving

stable motion trace and three other traces representing erratic motion, continuous drift and large high-frequency motion, were selected. For liver, we selected traces exhibiting large translational and rotational motion caused by diaphragm movement. For lung, the selected traces exhibited large translational AP motion, large rotational motion along the SI axis, and large translational motion along the SI axis. The prostate and liver traces were previously recorded using KIM and the lung traces were recorded using the Calypso motion tracking system.

Several pre-processing steps were applied to the motion traces. The prostate traces were pre-processed to reverse any gated couch shifts during treatment due to the large motion of the target. The liver and lung traces were shifted so that the mean motion in each axis was initially zero for the first 20 seconds. This simulated a setup in which the patient was centered with the mean target position at the treatment isocenter. Since the original liver motion was recorded for only 60 seconds, three repetitions of this trace were stitched together to generate a 3 min sequence required for the dynamic localization accuracy tests. Finally, the selected traces were filtered to remove measurement noise produced by the KIM and Calypso systems and to ensure smooth motion of the phantom, which is more representative of real physiological tumor motion. Filtering was performed by measuring the measurement jitter from each system and calculating the periodogram, an estimate of the spectral density of the measurement data (Smith 1999). A custom low pass filter was then determined based on the cut-off frequencies outside the measurement (signal) frequency, thereby retaining relevant motion frequencies related to breathing and heartbeat. The filter was a 20th order equiripple Finite Impulse Response (FRI) low pass filter with the corner frequency of 1 Hz and a stop-band frequency of 2 Hz for signal. The attenuation at the stop-band frequency was -40dB.

Once the robotic motion system was aligned to the radiotherapy coordinate reference frame, the Calypso tracking system was set up to sample motion at 25 Hz and the test trace was executed. The Calypso data were filtered to remove measurement jitter using the same low pass filter applied to the tumor motion traces. Finally, the data were transformed from the robot global coordinate system to the radiotherapy coordinate system. The input motion traces were then compared with the recorded motion from the Calypso system. Synchronization of the robot and Calypso data was achieved by manually aligning the traces at the initial transition of the phantom from stationary to moving. Since the Calypso motion tracking system only records translational motion in real-time, the position information for the three markers were post-processed offline to determine the rotational motion in the LR, SI and AP directions based on a pose estimation method using the iterative closest point algorithm (Tehrani *et al* 2013).

3. Results

3.1. System repeatability

Table 1 shows the repeatability of setting up and running motion traces using the system. Repeatability is reported conservatively as the maximum standard deviation across the 4 trials for each motion trace, and across all samples. In all cases the repeatability was better than 0.5 deg and 0.3 mm for rotation and translation, respectively. Repeatability here is reported with respect to the robot coordinate system.

Table 1. The system repeatability over 4 trials. Values are the maximum standard deviation (mm and deg) across 4 trials and all samples.

	x (mm)	y (mm)	z (mm)	x-rot (°)	y-rot (°)	z-rot (°)
Prostate	0.26	0.19	0.22	0.41	0.16	0.17
Liver	0.24	0.09	0.14	0.07	0.07	0.09
Lung	0.13	0.10	0.15	0.09	0.10	0.11

3.2. Static localization accuracy

Table 2 shows the static localization accuracy of the robotic motion system. The mean discrepancy in pose between the robotic phantom and Calypso for the LR, SI and AP axes was 0.09 mm, 0.08 mm and 0.02 mm for translations, and 0.20°, 0.06° and 0.06° for rotations, respectively.

3.3. Dynamic localization accuracy

The robotic motion input and the recorded Calypso motion of the tumor trajectories for both translation and rotation are shown in figures 4, 5 and 6 for the prostate, liver and lung traces, respectively. In each case, a 60-second snippet of the measured motion trace is shown to illustrate the alignment of the two datasets. The dynamic localization accuracy of the robotic motion system was computed as the root mean square error (RMSE) and the difference between the commanded robot pose and measured Calypso pose for each component of motion (table 3). Quantitatively, the mean RMSE for the LR, SI and AP directions was 0.13 mm, 0.16 mm and 0.15 mm for x, y and z translations, respectively, and 0.57°, 0.46° and 0.32° for x, y and z rotations, respectively. The mean difference in the LR, SI and AP directions was -0.02 mm, -0.03 mm and 0.03 mm for translations, respectively, and -0.06°, 0.03° and 0.01° for rotations, respectively.

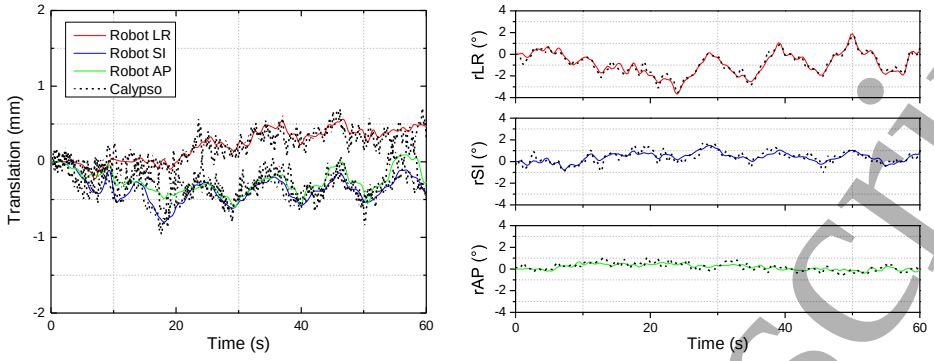

(a) Prostate stable: translation (b) Prostate stable: rotation

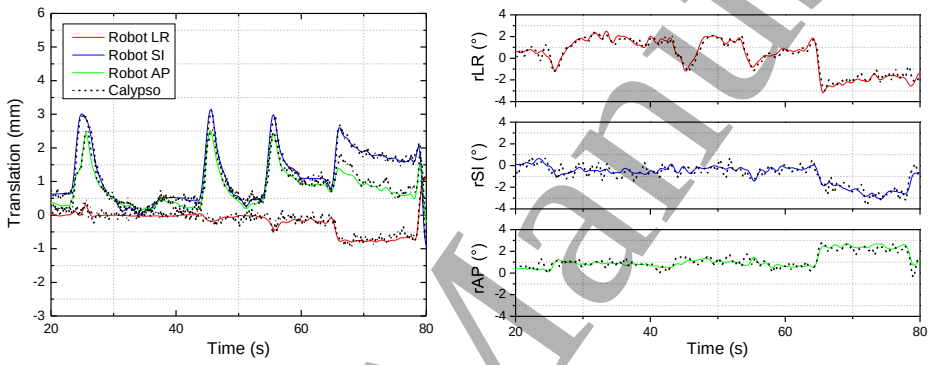

(c) Prostate erratic: translation (d) Prostate erratic: rotation

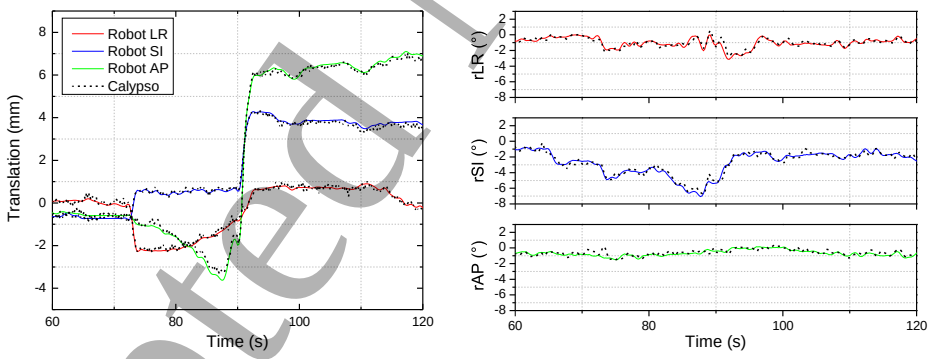

(e) Prostate persistent excursion: translation (f) Prostate persistent excursion: rotation

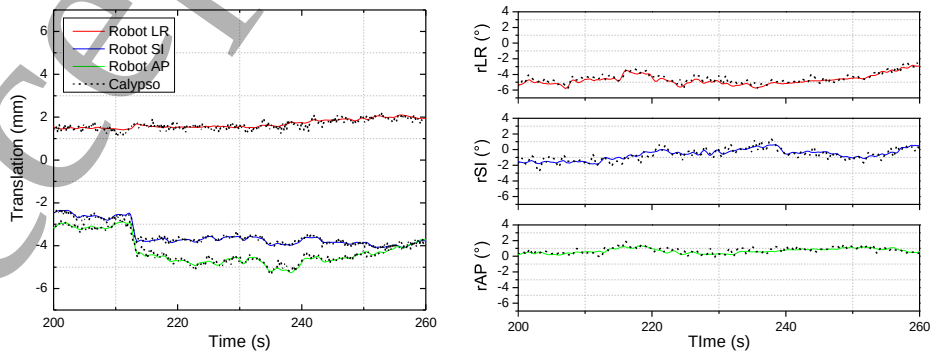

(g) Prostate continuous: translation (h) Prostate continuous: rotation

Figure 4. Prostate motion 6DoF dynamic localization accuracy. The input robot motion is shown as red, blue and green for LR, SI and AP directions, respectively. The Calypso motion output is represented as black dashed lines.

Table 2. Static localization accuracy, showing the commanded robot position (input) versus the average measured Calypso position and standard deviation (SD).

	Commanded robot position	Calypso	SD
LR (mm)	+40	40.13	0.03
	-40	-40.07	0.05
SI (mm)	+40	40.14	0.02
	-40	-40.02	0.02
AP (mm)	+40	40.02	0.04
	-40	-40.02	0.01
rLR (°)	+10	10.04	0.21
	-10	-9.69	0.21
rSI (°)	+10	10.02	0.13
	-10	-10.07	0.06
rAP (°)	+10	9.98	0.14
	-10	-9.92	0.49

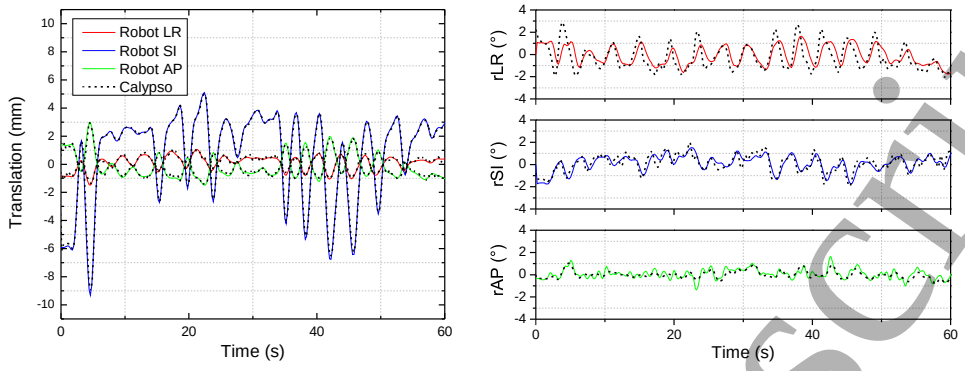

(a) Liver small: translation (b) Liver small: rotation

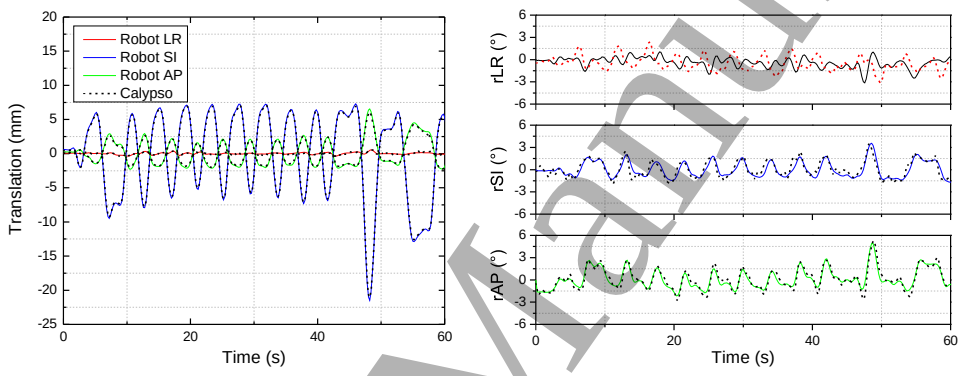

(c) Liver large: translation (d) Liver large: rotation

Figure 5. Liver motion 6DoF dynamic localization accuracy. The input robot motion is shown as red, blue and green for LR, SI and AP directions, respectively. The Calypso motion output is represented as black dashed lines.

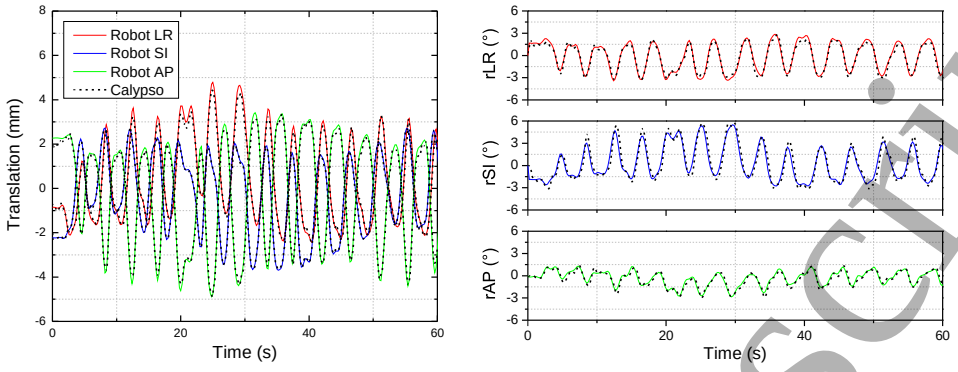

(a) Lung large: translation (b) Lung large: rotation

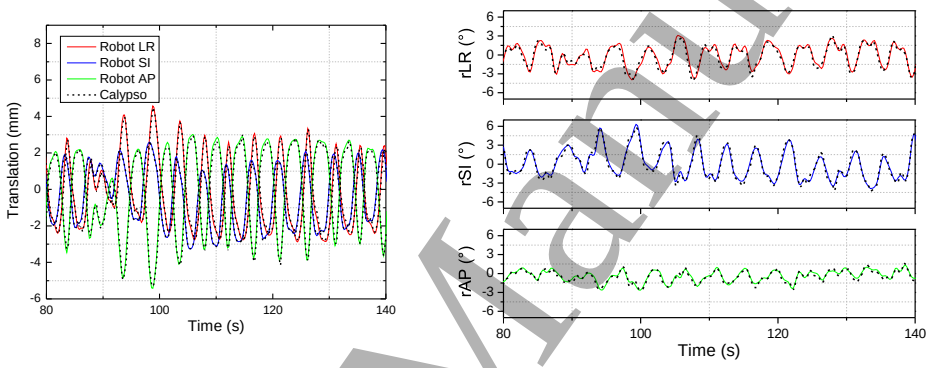

(c) Lung small: translation (d) Lung small: rotation

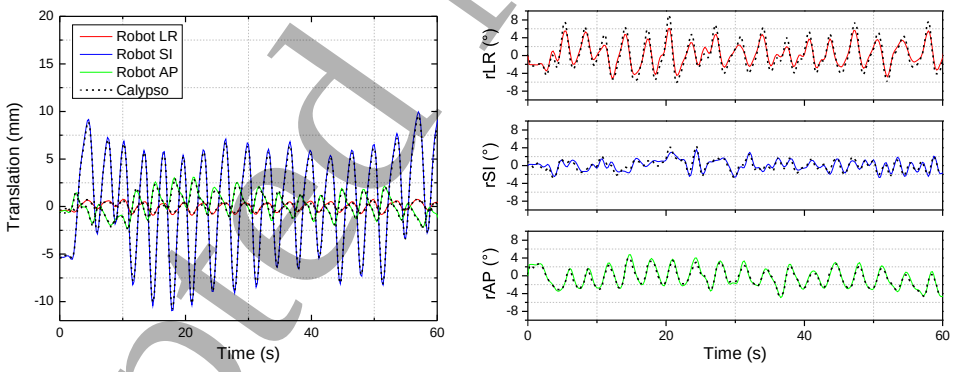

(e) Lung large: translation (f) Lung large: rotation

Figure 6. Lung motion 6DoF dynamic localization accuracy. The input robot motion is shown as red, blue and green for LR, SI and AP directions, respectively. The Calypso motion output is represented as black dashed lines.

Table 3. The dynamic localization accuracy of the robotic motion system expressed as the mean difference, SD and RMSE between the input robot motion and Calypso motion.

	Mean difference	SD	RMSE
LR (mm)	-0.02	0.12	0.13
SI (mm)	-0.03	0.15	0.16
AP (mm)	-0.03	0.14	0.15
rLR (°)	-0.06	0.56	0.57
rSI (°)	0.03	0.46	0.46
rAP (°)	0.01	0.30	0.32

4. Discussion

We have developed a 6DoF robotic motion system and characterised its performance for potential use in geometric QA for IGRT. The system combines a commercially available 6-axis robot with a custom-designed phantom and motion control algorithm, thereby enabling reproducible manipulation of the phantom according to commanded motion sequences representing real tumour trajectories. For this work, the phantom only contained embedded Calypso markers so that we could benchmark the accuracy of the system. In practice, however, the phantom would additionally have an embedded detector for complete dosimetric QA of motion-adaptive radiation therapy techniques.

Our results show that executed sequences from multiple independent set-ups of our system are highly repeatable (Table 1). This is despite the current requirement of a manual step to align the phantom to the treatment room lasers. The repeatability measurements reported in Table 1 are with respect to the robot's native coordinate system and do not include the UR3 intrinsic positional repeatability of 100 μm. (Note that intrinsic repeatability refers to the precision with which the robot returns to a specified position.) Taking the intrinsic repeatability into account, the overall repeatability of motion sequences using our system was <0.28 mm.

Robot manufacturers do not typically report accuracy, only repeatability. Therefore, it was important to benchmark the accuracy of motion commanded by our system against a well validated ground-truth system used in the radiotherapy context. The static and dynamic localization accuracy of the Calypso system is <0.5 mm and 0.33 mm, respectively (Santanam *et al* 2008), and the reported rotational accuracy is 0.1° ±0.7° (max 1°) (Santanam *et al* 2009). Therefore, the accuracy is within the 1 mm/1° positional tolerances for linear accelerators stated in AAPM TG-142 protocol (Klein *et al* 2009*a*).

The static and dynamic accuracy of our system was within the 0.5 mm variance of the Calypso system (Systems 2013). It is worth noting that because the Calypso motion tracking system is based on tracking electromagnetic markers, the marker localization accuracy can be affected by metallic distortion (Franz *et al* 2014). Thus, the metal in the robotic arm may have added additional discrepancies in the geometric agreement between the robotic motion system and the Calypso system.

Lung and liver motion traces, which exhibit large directional changes and large accelerations relative to other tumour trajectories (e.g. prostate), provided a good test of the dynamic geometric accuracy of the robotic motion system. The phantom mapped out these traces with a geometric accuracy <0.2 mm and <0.6° for translation and rotation, respectively. The translational accuracy of the robotic motion system reported here is slightly poorer than a 4DoF motion phantom (0.1 mm), developed by Nobutaka et al. for patient-specific QA of surrogate tracking in IMRT (Mukumoto *et al* 2016). The accuracy of the robotic motion system is also slightly worse than that of the commercially available 5DoF Hexamotion system (0.1 mm and 0.1° for translation and rotation respectively (Huang *et al* 2017)). However, the robotic system has the advantage of an additional degree-of-freedom and a considerably larger range of motion in all axes.

The larger RMSE for rotation is a by-product of both the transponder locations and the method used to compute rotation. Translations can be easily compared based on the individual transponder locations, with relatively smaller error contributions. Rotations on the other hand are computed based on changes in the combined transponder locations, each of which contributes some error. The arrangement of locations also impacts the accuracy of rotation estimation – the closer, or more collinear, the distribution, the greater the ambiguity and error. These aspects are manifest in the rotation results. However, given the range of motion that was tracked, the accuracy values were encouraging and indicate that the system is modelling real physiological traces extremely well.

Although we used embedded electromagnetic markers in order to benchmark our system against the Calypso, alternate phantoms with X-ray visible markers for Cyberknife, Vero and conventional linac real-time guidance methods (Keall *et al* 2018) could also be considered. Moreover, phantoms with lung inserts rather than markers could be developed for markerless tracking applications (Awano *et al* 2017, Tanaka *et al* 2015, Shieh *et al* 2017). These phantom designs will be the focus of future work.

As mentioned above, the current robotic motion system was designed only for geometric validation - no dosimetry has been investigated here. Thus, the next stage of development will be concurrent geometric and dosimetric QA measurements by integrating a radiation detector (e.g. EBT3 film or detector arrays) into the phantom. An important constraint in the development of such a detector is the maximum payload limit of 3 kg for the UR3. The current phantom weighs approximately 2.3 kg, so we

expect that after replacing some of the PMMA with a dosimetry detector, it is very feasible to keep the total weight to <3 kg.

One final extension of the present work which would simplify implementing the method in practice is the automation of the phantom alignment to the treatment room lasers using an optical control loop.

5. Conclusion

We have developed a robotic system to accurately mimic both translational and rotational patient tumor motion. This device can perform geometric QA for 6DoF IGRT. The geometric accuracy of the 6DoF robotic motion system was characterized using a commercially available clinical tracking system.

6. Acknowledgments

This work was supported by an Australian Government NHMRC Senior Principal Research Fellowship and a grant awarded through the 2014 round of the Priority-driven Collaborative Cancer Research Scheme and funded by Cancer Australia.

References

ACRF Image X Institute, Tumour motion (prostate, liver and lung) n.d. `http://sydney.edu.au/medicine/image-x/public-data/6dof-tumour.php`. Accessed: 2018-05-22.

Awano N, Ikushima S, Izumo T, Tone M, Fukuda K, Miyamoto S, Bae Y, Kumasaka T, Terada Y, Furuhata Y, Nomura R and Sato K 2017 Efficacy and safety of stereotactic body radiotherapy using cyberknife in stage i primary lung tumor *Japanese Journal of Clinical Oncology* **47**(10), 969–975.

Bajd T, Mihelj M, Lenarčič J, Stanovnik A and Munih M 2010 *Robotics* Springer.

Belcher A H, Liu X, Chmura S, Yenice K and Wiersma R D 2017 Towards frameless maskless srs through real-time 6dof robotic motion compensation *Physics in Medicine & Biology* **62**(23), 9054.

Belcher A H, Liu X, Grelewicz Z, Pearson E and Wiersma R D 2014 Development of a 6dof robotic motion phantom for radiation therapy *Medical Physics* **41**(12), 121704.

Bell L J, Eade T, Kneebone A, Hruby G, Alfieri F, Bromley R, Grimberg K, Barnes M and Booth J T 2017 Initial experience with intra-fraction motion monitoring using calypso guided volumetric modulated arc therapy for definitive prostate cancer treatment. *Journal Of Medical Radiation Sciences* **64**(1), 25 – 34.

Commission I E 2011 Radiotherapy equipment - coordinates, movements and scales Technical report International Electrotechnical Commission (IEC).

Depuydt T, Poels K, Verellen D, Engels B, Collen C, Buleteanu M, den Begin R V, Boussaer M, Duchateau M, Gevaert T, Storme G and de Ridder M 2014 Treating patients with real-time tumor tracking using the vero gimbaled linac system: implementation and first review. *Radiotherapy and oncology : journal of the European Society for Therapeutic Radiology and Oncology* **112 3**, 343–51.

Ehrbar S, Jöhl A, Tartas A, Stark L S, Riesterer O, Kloeck S, Guckenberger M and Tanadini-Lang S 2017 Itv, mid-ventilation, gating or couch tracking - a comparison of respiratory motion-

management techniques based on 4d dose calculations. *Radiotherapy and oncology : journal of the European Society for Therapeutic Radiology and Oncology* **124 1**, 80–88.

Falk M, af Rosenschöld P M, Keall P, Cattell H, Cho B C, Poulsen P, Povzner S, Sawant A, Zimmerman J and Korreman S 2010 Real-time dynamic mlc tracking for inversely optimized arc radiotherapy *Radiotherapy and Oncology* **94**(2), 218 – 223. Selected papers from the 10th Biennial ESTRO Conference on Physics and Radiation Technology for Clinical Radiotherapy.

Franz A M, Schmitt D, Seitel A, Chatrasingh M, Echner G, Oelfke U, Nill S, Birkfellner W and Maier-Hein L 2014 Standardized accuracy assessment of the calypso wireless transponder tracking system *Physics in Medicine & Biology* **59**(22), 6797.
URL: *http://stacks.iop.org/0031-9155/59/i=22/a=6797*

Galal M, Rahill C and Connolly J 2016 Preparations for the implementation of cyberknife lung sbrt *Physica Medica* **32**(7), 957.

Gevaert T, Verellen D, Engels B, Depuydt T, Heuninckx K, Tournel K, Duchateau M, Reynders T and Ridder M D 2012 Clinical evaluation of a robotic 6-degree of freedom treatment couch for frameless radiosurgery *International Journal of Radiation Oncology*Biology*Physics* **83**(1), 467 – 474.

Huang C Y, Keall P, Rice A, Colvill E, Ng J A and Booth J T 2017 Performance assessment of a programmable five degrees-of-freedom motion platform for quality assurance of motion management techniques in radiotherapy *Australasian Physical & Engineering Sciences in Medicine* **40**(3), 643–649.

Huang C Y, Tehrani J N, Ng J A, Booth J and Keall" P 2015 Six degrees-of-freedom prostate and lung tumor motion measurements using kilovoltage intrafraction monitoring *International Journal of Radiation Oncology*Biology*Physics* **91**(2), 368 – 375.

Keall P J, Aun Ng J, O'Brien R, Colvill E, Huang C Y, Rugaard Poulsen P, Fledelius W, Juneja P, Simpson E, Bell L, Alfieri F, Eade T, Kneebone A and Booth J T 2015 The first clinical treatment with kilovoltage intrafraction monitoring (kim): A real-time image guidance method *Medical Physics* **42**(1), 354–358.

Keall P J, Colvill E, O'Brien R, Ng J A, Poulsen P R, Eade T, Kneebone A and Booth J T 2016 The first clinical implementation of electromagnetic transponder-guided mlc tracking *Medical Physics* **41**(2), 020702.

Keall P, Nguyen D, O'Brien R, Zhang P, Happersett L, Bertholet J and Poulsen P 2018 A review of real-time 3d igrt on standard-equipped cancer radiotherapy systems: Are we at the tipping point for the era of real-time radiotherapy? *International Journal of Radiation Oncology Biology Physics* .

Klein E E, Hanley J, Bayouth J, Yin F F, Simon W, Dresser S, Serago C, Aguirre F, Ma L, Arjomandy B, Liu C, Sandin C and Holmes T 2009*a* Task group 142 report: Quality assurance of medical acceleratorsa) *Medical Physics* **36**(9Part1), 4197–4212.

Klein E E, Hanley J, Bayouth J, Yin F, Simon W, Dresser S, Serago C, Aguirre F, Ma L, Arjomandy B, Liu C, Sandin C and Holmes T 2009*b* Task group 142 report: Quality assurance of medical acceleratorsa) *Medical Physics* **36**(9Part1), 4197–4212.

Kupelian P, Willoughby T, Mahadevan A, Djemil T, Weinstein G, Jani S, Enke C, Solberg T, Flores N, Liu D, Beyer D and Levine L 2007 Multi-institutional clinical experience with the calypso system in localization and continuous, real-time monitoring of the prostate gland during external radiotherapy *International Journal of Radiation Oncology*Biology*Physics* **67**(4), 1088 – 1098.

Kutcher G J, Coia L, Gillin M, Hanson W F, Leibel S, Morton R J, Palta J R, Purdy J A, Reinstein L E, Svensson G K, Weller M and Wingfield L 1994 Comprehensive qa for radiation oncology: Report of aapm radiation therapy committee task group 40 *Medical Physics* **21**(4), 581–618.

Mukumoto N, Nakamura M, Yamada M, Takahashi K, Akimoto M, Miyabe Y, Yokota K, Kaneko S, Nakamura A, Itasaka S, Matsuo Y, Mizowaki T, Kokubo M and Hiraoka M 2016 Development of a four-axis moving phantom for patient-specific qa of surrogate signal-based tracking imrt *Medical Physics* **43**(12), 6364–6374.

Mutic S and Dempsey J F 2014 The viewray system: Magnetic resonance–guided and controlled radiotherapy *Seminars in Radiation Oncology* **24**(3), 196 – 199. Magnetic Resonance Imaging in Radiation Oncology.

Plathow C, Schoebinger M, Fink C, Hof H, Debus J, Meinzer H P and Kauczor H U 2006 Quantification of lung tumor volume and rotation at 3d dynamic parallel mr imaging with view sharing: Preliminary results **240**, 537–45.

Robots U 2015 Ur3 technical specifications item no. 110103 Technical report.

Santanam L, Malinowski K, Hubenshmidt J, Dimmer S, Mayse M L, Bradley J, Chaudhari A, Lechleiter K, Goddu S K M, Esthappan J, Mutic S, Low D A and Parikh P 2008 Fiducial-based translational localization accuracy of electromagnetic tracking system and on-board kilovoltage imaging system *International Journal of Radiation Oncology*Biology*Physics* **70**(3), 892 – 899.

Santanam L, Noel C, Willoughby T R, Esthappan J, Mutic S, Klein E E, Low D A and Parikh P J 2009 Quality assurance for clinical implementation of an electromagnetic tracking system *Medical Physics* **36**(8), 3477–3486.

Schmidhalter D, Fix M K, Wyss M, Schaer N, Munro P, Scheib S, Kunz P and Manser P 2013 Evaluation of a new six degrees of freedom couch for radiation therapy *Medical Physics* **40**(11), 111710–n/a. 111710.

Schmidhalter D, Malthaner M, Born E J, Pica A, Schmuecking M, Aebersold D M, Fix M K and Manser P 2014 Assessment of patient setup errors in igrt in combination with a six degrees of freedom couch *Zeitschrift für Medizinische Physik* **24**(2), 112 – 122.

Shieh C C, Caillet V, Dunbar M, Keall P J, Booth J T, Hardcastle N, Haddad C, Eade T and Feain I 2017 A bayesian approach for three-dimensional markerless tumor tracking using kv imaging during lung radiotherapy *Physics in Medicine & Biology* **62**(8), 3065.

Shieh C C, Keall P J, Kuncic Z, Huang C Y and Feain I 2015 Markerless tumor tracking using short kilovoltage imaging arcs for lung image-guided radiotherapy *Physics in Medicine & Biology* **60**(24), 9437.

Smith S W 1999 *The Scientist and Engineer's Guide to Digital Signal Processing* California Technical Publishing.

Sörnsen de Koste J R, Dahele M, Mostafavi H, Sloutsky A, Senan S, Slotman B J and Verbakel W F A R 2015 Markerless tracking of small lung tumors for stereotactic radiotherapy *Medical Physics* **42**(4), 1640–1652.

Systems V M 2013 Calypso system operator's manual version 3.0 Technical report Varian Medical Systems.

Tanaka R, Sanada S, Sakuta K and Kawashima H 2015 Improved accuracy of markerless motion tracking on bone suppression images: preliminary study for image-guided radiation therapy (igrt) *Physics in Medicine & Biology* **60**(10), N209.

Tehrani J N, O'brien R T, Poulsen P R and Keall P J 2013 Real-time estimation of prostate tumor rotation and translation with a kv imaging system based on an iterative closest point algorithm. *Physics in medicine and biology* **58 23**, 8517–33.

Universal Robots, "Modbus Server - 16377" n.d. `https://www.universal-robots.com/how-tos-and-faqs/how-to/ur-how-tos/modbus-server-16377/`. Published: 2015, Accessed: 2018-10-17.

Wilbert J, Baier K, Hermann C, Flentje M and Guckenberger M 2013 Accuracy of real-time couch tracking during 3-dimensional conformal radiation therapy, intensity modulated radiation therapy, and volumetric modulated arc therapy for prostate cancer *International Journal of Radiation Oncology*Biology*Physics* **85**(1), 237 – 242.